

Integrated 3D-printed reactionware for chemical synthesis and analysis

Mark D. Symes^{1†}, Philip J. Kitson^{1†}, Jun Yan^{1†}, Craig J. Richmond¹, Geoffrey J. T. Cooper¹, Richard W. Bowman², Turlif Vilbrandt³ and Leroy Cronin^{1*}

Three-dimensional (3D) printing has the potential to transform science and technology by creating bespoke, low-cost appliances that previously required dedicated facilities to make. An attractive, but unexplored, application is to use a 3D printer to initiate chemical reactions by printing the reagents directly into a 3D reactionware matrix, and so put reactionware design, construction and operation under digital control. Here, using a low-cost 3D printer and open-source design software we produced reactionware for organic and inorganic synthesis, which included printed-in catalysts and other architectures with printed-in components for electrochemical and spectroscopic analysis. This enabled reactions to be monitored *in situ* so that different reactionware architectures could be screened for their efficacy for a given process, with a digital feedback mechanism for device optimization. Furthermore, solely by modifying reactionware architecture, reaction outcomes can be altered. Taken together, this approach constitutes a relatively cheap, automated and reconfigurable chemical discovery platform that makes techniques from chemical engineering accessible to typical synthetic laboratories.

The use of three-dimensional (3D) printing technologies by individuals promises to bypass sophisticated manufacturing centres and revolutionize every part of the way that materials are turned into functional devices, from design through to operation^{1,2}. However, apart from the utilization of 3D printing for tissue-growth scaffolds^{3–6} and large-scale industrial prototyping⁷, applications of this technology remain limited. Recently, 3D printing was applied to produce highly specialized electronic⁸, microfluidic⁹ and pneumatic^{10,11} devices, and yet the potential for using 3D-printed reactors as accessible and readily reconfigurable chemical discovery tools has not been addressed.

Motivated by the idea of a future whereby users can download a design for a product from the internet, modify it to suit an intended purpose and then rapidly produce any number of such items at low cost on a portable, robust device¹², we developed strategies to produce integrated 3D-printer/design-software/chemistry packages whereby individuals could one day have access to chemistry and chemical discovery without the need for expensive laboratory infrastructures. This would not only place traditionally expensive chemical engineering technology within reach of typical laboratories and small commercial enterprises¹³, but also could revolutionize access to healthcare and the chemical sciences in general in the developing world^{14,15} and so allow diagnosis and treatment preparation to occur in a sustainable, decentralized and timely fashion. With this in mind, we opted to use flexible direct-writing (or ‘robocasting’)^{16–18} 3D printing technologies (whereby a robotically controlled syringe deposits gels at room temperature, which subsequently set without the need for heat or chemical curing steps) that combine low printer-hardware costs with a comparatively broad range of potential printable materials.

Herein, we demonstrate the use of the low-cost (US\$2,000, NextFab Store) Fab@Home^{19,20} robocasting platform (Fig. 1a,b) for the automated production of self-healing, reusable and robust reactionware for both synthesis and spectroscopy. All the

parameters regarding the dimensions of these devices could be adjusted digitally during the computer-aided design process with great ease, and subsequent printing could be automated effectively. This made iterative design and manufacture straightforward, and exploited the inherent reconfigurability of the system to link reactor design to chemical discovery. Hence, we were able to develop architectures conducive to (1) the formation and crystallization of two new inorganic nanoclusters of formula $(C_2H_8N)_mNa_n[W_{19}M_2O_{61}Cl(SeO_3)_2(H_2O)_2]Cl_2 \cdot xH_2O$ (where $M = Co(II)$ (1) or $Mn(II)$ (2)); (2) the synthesis of the previously unreported organic heterocyclic compound $C_{21}H_{17}BrN_2O$ (3) and (3) conducting real-time *in situ* spectroelectrochemistry during the reduction of phosphomolybdic acid (PMA). More importantly, we were able to switch completely the outcome of the reaction of 4-methoxyaniline with 5-(2-bromoethyl)phenanthridinium bromide^{21,22} (from 80% $C_{22}H_{20}N_2O$ (4) to >90% $C_{22}H_{19}BrN_2O$ (5)) on alteration of the reactor architecture, without altering any of the other reaction conditions.

Modification of reactor design to produce a certain reaction outcome is an established practice in large-scale chemical engineering but, until now, such techniques were essentially inaccessible to typical laboratories and small companies on account of cost and complexity. Moreover, we were also able to demonstrate the potential for ‘printing-in’ catalysts into the structure of the reactionware, which opens up the possibility of creating multifunctional bespoke reactionware for applications across chemistry. Thus, we show how coupling digital design technology with 3D printing makes ‘reactionware space’ a parameter that can be optimized systematically to drive chemical reactions towards the desired products.

Results and discussion

The bespoke multifunctional reactionware (Fig. 1c and Supplementary Figs S5–S7) was designed using the Rhino3d software package²³ and subsequently uploaded to a Fab@Home

¹WestCHEM, School of Chemistry, The University of Glasgow, University Avenue, Glasgow G12 8QQ, UK, ²School of Physics & Astronomy, Kelvin Building, The University of Glasgow, University Avenue, Glasgow G12 8QQ, UK, ³Uformia AS, Industriveien 6, 9062 Furufelaten, Norway; [†]These authors contributed equally to this work. *e-mail: Lee.Cronin@glasgow.ac.uk

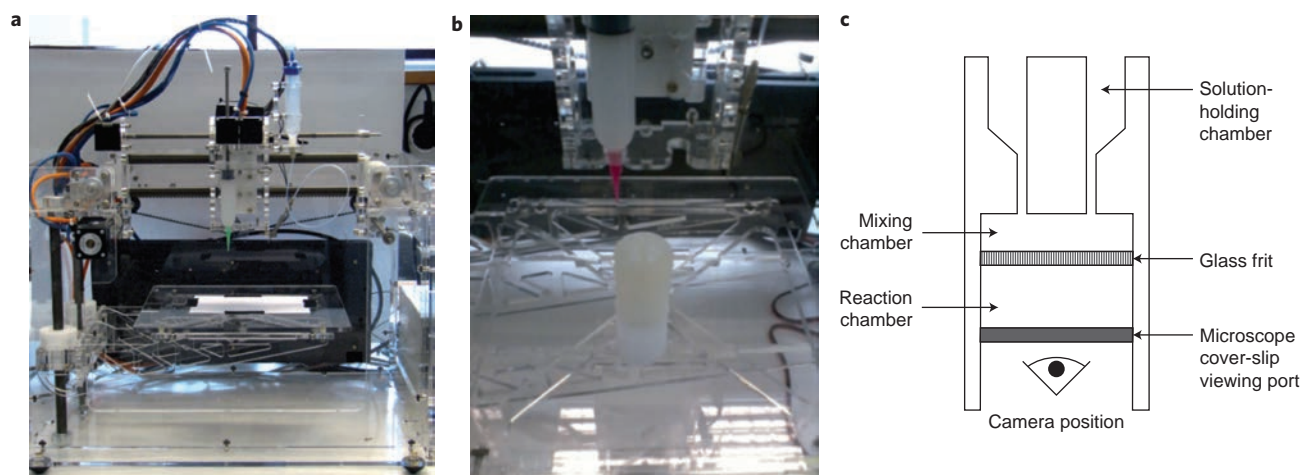


Figure 1 | The Fab@Home Version 0.24 RC6 freeform fabricator. **a**, The fabricator viewed from the front, with a single syringe of acetoxy silicone polymer loaded in the printing head. The white area below the printing head is a square of ordinary paper onto which the reactionware was printed. **b**, The fabricator printing one of the devices used in this work. **c**, Schematic of the as-printed multipurpose reactionware used in the synthesis of compounds **1–3**, which shows the key features of the design.

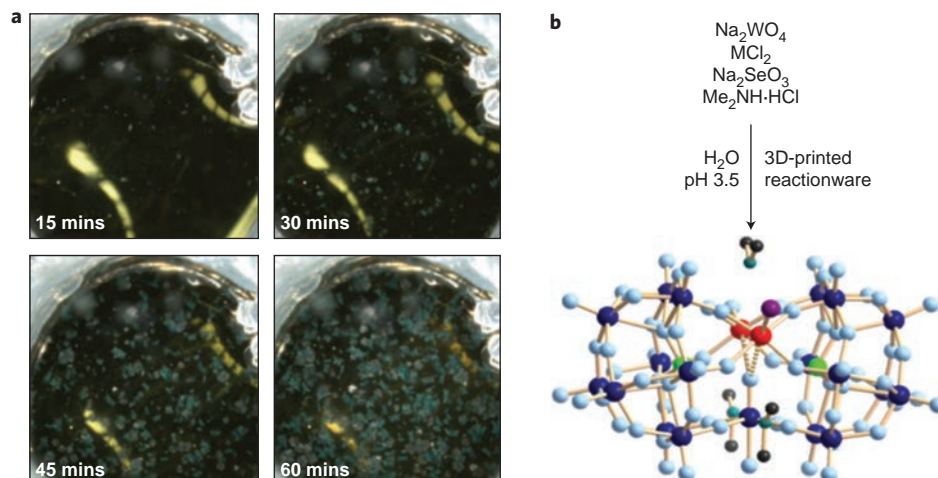


Figure 2 | The synthesis and crystallization of polyoxometalates in the 3D-printed reactionware. **a**, Photographs of the crystallization of $(C_2H_8N)_7Na_4[W_{19}Co_2O_{61}Cl(SeO_3)_2(H_2O)_2]Cl_2 \cdot 6H_2O$ at various times after the initial mixing. **b**, Synthesis and ball-and-stick representation of the structure of $((C_2H_8N)_3[W_{19}M_2O_{61}Cl(SeO_3)_2(H_2O)_2])^{6-}$ ($M = Co(II)$ or $Mn(II)$). Protons are omitted for clarity. Black, teal, cyan, green, violet, dark blue and red represent C, N, O, Se, Cl, W and M, respectively.

platform assembled in the laboratory. The device was then printed using a robust, quick-curing acetoxy silicone polymer (Loctite 5366 bathroom sealant, LOCTITE) as the primary material and inserting the non-printable components (glass frit and microscope slide/indium tin oxide (ITO) viewing window) during pre-programmed pauses in the printing schedule (see Supplementary Information for details)²⁴.

This device was then used for the inorganic nanocluster assembly. An aqueous solution of $CoCl_2$ was printed (that is, dispensed by the printer) into one solution-holding chamber and an acidic solution of the dilacurary polyoxotungstate $[Se_2W_{19}O_{67}(H_2O)]^{12-}$ (prepared using an adapted literature procedure²⁵) was printed into the other holding chamber (see Supplementary Information). The two solutions remained in their respective chambers and did not flow into the mixing chamber until induced to do so. To this end, a needle attached to a vacuum source was inserted through the wall of the reaction chamber to suck the two solutions into the mixing chamber, through the frit and into the lower reaction chamber at a controlled rate. On removal of the needle, the walls

of the reaction chamber resealed spontaneously, making the chamber watertight. The subsequent crystallization events were monitored through the transparent viewing window incorporated into the device (see Supplementary Video S1). Figure 2a shows this crystallization process at various intervals.

Importantly, once the precursor solutions had passed into the mixing chamber, the whole device could be held upside-down and shaken repeatedly without any leakage of the solutions. When crystals of a suitable size had formed (typically within 10–60 minutes) the crystallization device was cut in half with a scalpel and the crystals were removed and analysed by X-ray crystallography, Fourier transform infrared spectroscopy, thermogravimetric analysis and elemental analysis (see Supplementary Information). The crystal structure of **1** (Fig. 2b) contains a classic sandwich-type²⁵ anionic cluster $[W_{19}Co_2O_{61}Cl(SeO_3)_2(H_2O)_2]^{9-}$ formed of two trilacurary $[W_9O_{30}(SeO_3)]^{8-}$ building blocks (average Se–O bond length = 1.70(2) Å) and a central trigonal planar core. This core contains an octahedral WO_6 unit and two CoO_6 centres. One terminal oxo ligand of the WO_6 unit coordinates to both the

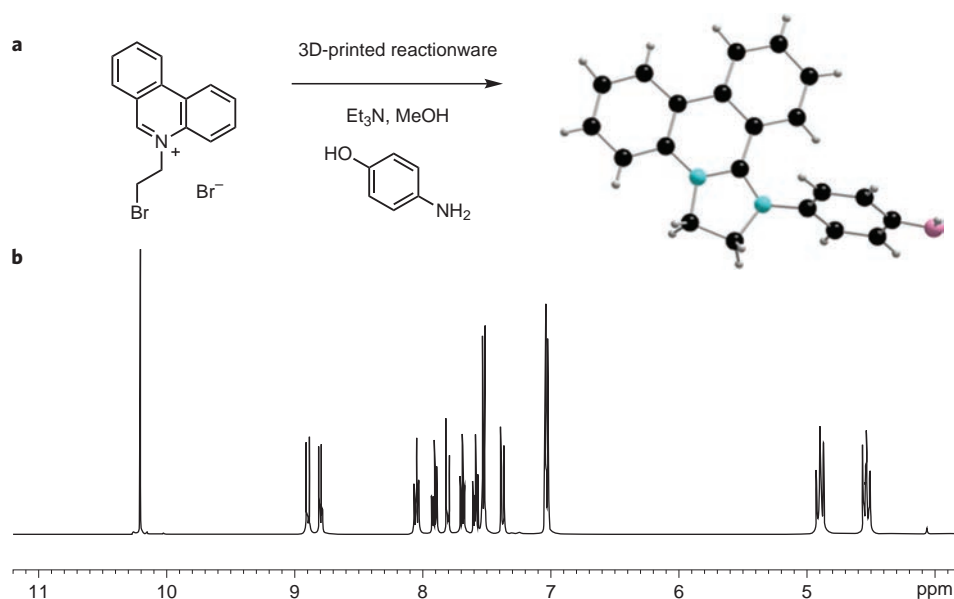


Figure 3 | The synthesis of heterocycle 3 in 3D-printed reactionware. **a**, Synthetic scheme with a ball-and-stick representation of the crystal structure of the organic phenanthridine-based heterocycle **3**. Grey, black, light blue and pink represent protons, C, N and O, respectively. **b**, The partial ^1H NMR spectrum (400 MHz, d_6 -DMSO, 298 K) of heterocycle **3**.

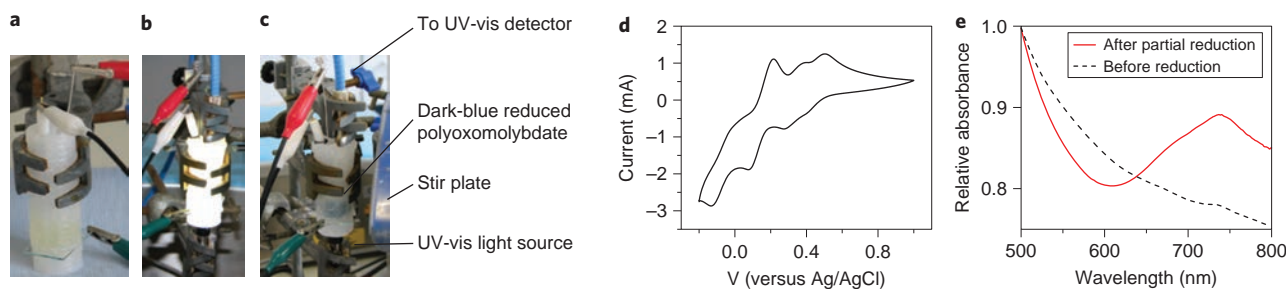


Figure 4 | The 3D-printed reactionware used for *in situ* spectroscopies. **a**, The reactionware as a cell for electrochemistry in a three-electrode configuration. **b, c**, The reactionware used for spectroelectrochemistry. **d**, Cyclic voltammetry, as recorded using the set-up shown in (a–c), for PMA (5 mM in 0.1 M H_2SO_4) at a scan rate of 0.1 V s^{-1} . **e**, Partial UV-vis spectrum obtained during the electrochemical cycling of the PMA solution. Relative absorbances are normalized at 500 nm. The active surface area of the ITO working electrode was 2.0 cm^2 . Black dashed line = before reduction, red solid line = after partial reduction.

CoO_6 units, and the terminal water ligand on one Co centre is substituted by a chloride. It is interesting that, in addition to a certain number of amines acting as cations and hydrogen bonding to the cluster, extra dimethyl ammonium ions are also disordered around the cluster in the crystal structure. Hence, we speculate that the excess of dimethyl ammonium hydrochloride accelerates the crystallization process (allowing single crystals to form in only a few minutes), whereas no single crystalline product can be isolated after a week if amines are absent.

The cleaved 3D-printed device was then washed with water and reconstituted by simply applying a thin layer of acetoxysilicone polymer to the cut edges, pressing the two halves of the device together by hand and then leaving it to set for an hour. Subsequently, it was reused successfully, as before, this time taking aqueous solutions of MnCl_2 and $[\text{Se}_2\text{W}_{19}\text{O}_{67}(\text{H}_2\text{O})]^{12-}$ to obtain crystals of formula $(\text{C}_2\text{H}_8\text{N})_8\text{Na}_3[\text{W}_{19}\text{Mn}_2\text{O}_{61}\text{Cl}(\text{SeO}_3)_2(\text{H}_2\text{O})_2]\text{Cl}_2 \cdot 6\text{H}_2\text{O}$ (**2**) (see Supplementary Information for details). Crystallographic unit-cell checks established that this compound had the same structure as compound **1** (see Supplementary Information).

Also, the same 3D-printed reactionware was found to be suitable for organic synthesis. Specifically, we synthesized the phenanthridine-based heterocycle **3** (see Fig. 3 and Supplementary

Information for experimental details and full characterization) by the reaction of 4-aminophenol, Et_3N and 5-(2-bromoethyl) phenanthridinium bromide in methanol (see Supplementary Information for a discussion of solvent compatibilities in the as-printed devices). On mixing in the 3D-printed reactionware, the reaction mixture turned an amber colour, and crystals of **3** suitable for X-ray diffraction were obtained from the liquor after 96 hours. The structure thus obtained is shown in Fig. 3, along with the ^1H NMR spectrum of compound **3** in d_6 -dimethylsulfoxide (DMSO).

Reactionware suitable for analytical and spectroscopic techniques could also be produced, which showcases the potential to monitor reactions *in situ* using such robocasting-fabricated devices. To this end, an adapted version of the reactionware shown in Fig. 1c was printed, whereby the frit was omitted and the microscope cover-slip viewing port replaced by a glass slide coated in a thin layer of the transparent conductor ITO, such that the ITO-coated surface faced into the reaction chamber. Initially, the central chamber of the device was charged with 2 ml of an aqueous 5 mM solution of PMA in 0.1 M H_2SO_4 . A thin Ag/AgCl reference electrode (white cable in Fig. 4a) and a Pt wire counter electrode (red cable) were then inserted into this solution through the pre-printed apertures between the solution-holding

chambers and the reaction chamber, and the ITO slide was connected to a potentiostat as the working electrode (green cable, see Fig. 4a).

Cycles from -0.2 V to $+1.0$ V and back to -0.2 V (versus Ag/AgCl) in this three-electrode set-up then produced the cyclic voltammogram in Fig. 4d, which shows four reversible redox processes centred at $+0.45$, $+0.30$, $+0.10$ and -0.10 V versus Ag/AgCl, in agreement with literature values²⁶. Moreover, on termination of the potential cycling at -0.2 V, the initially yellow solution had taken a slightly blue hue, characteristic of reduced polyoxomolybdates. We were able to use the configuration shown in Fig. 4b,c to monitor this colour change *in situ* by inserting a fibre-optic cable through one of the pre-printed holes in the top of the reactionware (the Pt counter electrode was moved and pushed through the resealable lid to make this possible), which was connected to the input port on a TIDAS ultraviolet-visible (UV-vis) spectrophotometer. The input light source was provided by a 150 W broad-spectrum Hg arc lamp, which was clamped below the apparatus such that the sample was irradiated from below, through the ITO window, during acquisition of the spectra. Comparison of the spectra obtained before and after the cyclic voltammogram (Fig. 4e) shows the appearance of a new broad peak centred around 750 nm, consistent with the slight bluish tinge now visible in the solution and with previous spectroelectrochemical studies on this compound²⁶. By equipping the reactionware with a small stir bar, the solution could be stirred magnetically (the stir plate was held to the side of the cell, see Fig. 4c). Hence, we were able to perform bulk electrolysis on the sample (the ITO working electrode was poised at -0.2 V versus the reference electrode), which led to the entire solution turning dark blue within a few minutes, a colour change clearly visible with the naked eye (see Fig. 4c). Such studies show that robocast 3D-printed reactionware is suitable for both spectroscopic analyses and bulk synthetic and electrochemical processes.

In addition to utilizing traditional electrodes within a 3D-printed cell, we were also able to 3D print entire electrochemical cells using the Fab@Home platform. For example, an acetoxysilicone polymer (before curing) was mixed with toluene to make a thinned gel, which was then mixed with conductive carbon black to produce a conductive paste suitable for loading into the 3D printer (see Supplementary Information and Supplementary Fig. S7 for details). A basic electrochemical cell was then produced, whereby two parallel lines of this conductive paste were printed onto a glass slide, about 0.5 cm apart, with the watertight housing of the cell being composed of unmodified acetoxysilicone bathroom sealant (see Fig. 5a). The glass slide was employed solely to aid visualization of the ensuing electrochemical reactions, and various functional architectures for electrochemical cells can be envisioned using solely printed components.

The two electrodes of the cell were then connected to a three-electrode potentiostat, as shown in Fig. 5b,c. The working electrode was connected to one rail of conductive paste using a copper wire and the reference and counter electrodes were both attached to the other rail of conductive paste to give a 'floating' reference configuration. The electrochemical cell was then filled with a 5 mM aqueous solution of PMA in 0.1 M H_2SO_4 , and a voltage of -2.5 V applied to the working electrode rail. Within a few minutes, the yellow polyoxometalate solution had started to turn blue around the working electrode as it was reduced. The reaction was followed visually (see Supplementary Video S2, which shows this process at 60 times the normal speed) and coulometrically (see Fig. 5d): the straight line of charge versus time obtained indicates that the cell was capable of supplying a constant current over the course of the experiment (>1 hour), which means that there was no obvious degradation in the conductivity of the cell over this time period.

Given the lack of constraints on what 'inks' could potentially be robocast printed (both in terms of the structural components of the

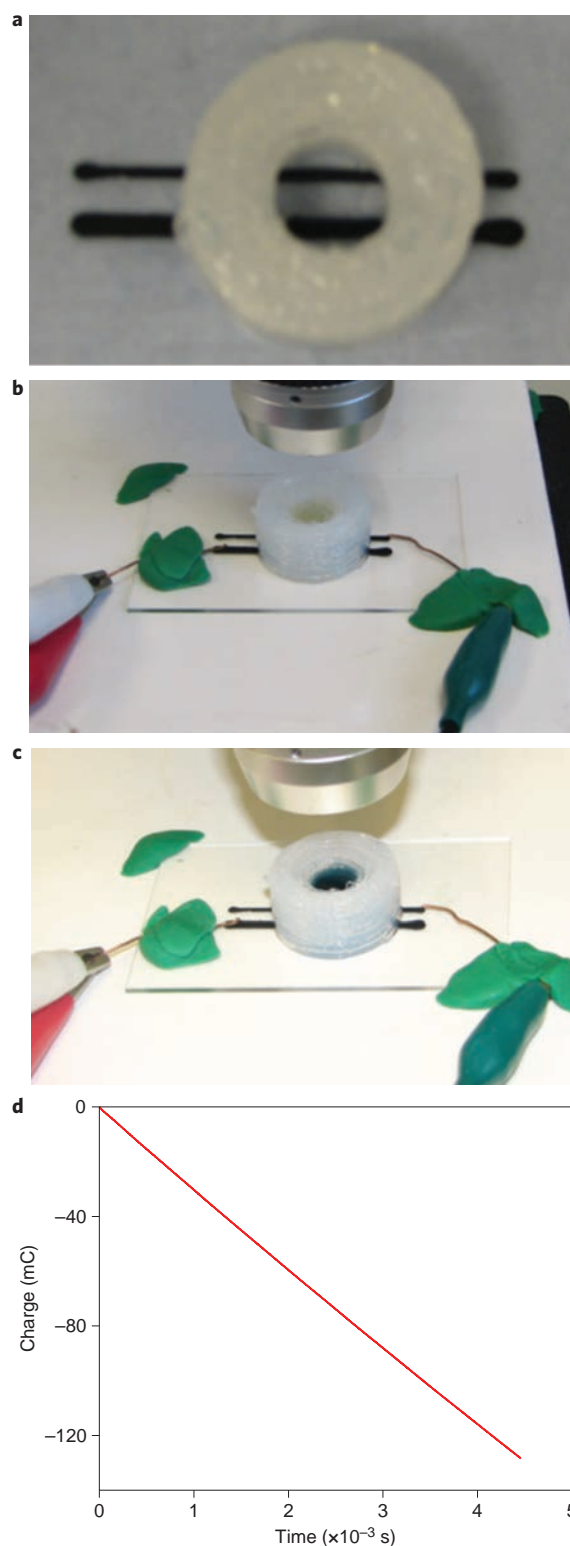


Figure 5 | The 3D-printed electrochemical cell and electrodes. **a**, The reactionware used for *in situ* spectroscopies showing the two conductive electrodes based on carbon black. The working electrode (upper line) had an area exposed to the reaction medium of approximately 0.8×0.1 cm² and the reference/counter electrode rail (lower line) had an exposed area of 1.0×0.2 cm². **b**, The connected cell filled with 1 ml of 5 mM PMA in 0.1 M H_2SO_4 before electrochemical reduction. **c**, The same cell after reduction at -2.5 V for 4,500 seconds. **d**, The charge passed versus time curve for the reduction process shows that the current was constant over the time course of the experiment.

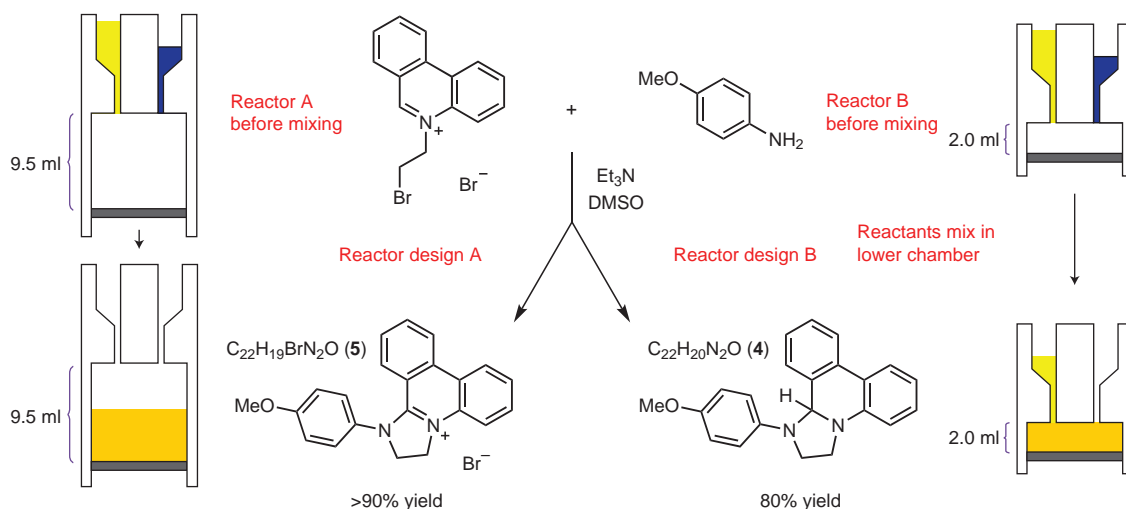


Figure 6 | The 3D-printed reactionware-assisted selective syntheses of $C_{22}H_{20}N_2O$ (4) and $C_{22}H_{19}BrN_2O$ (5). The outcome of the reaction can be switched between these two products by simply altering the reactor architecture. For Reactor A, both reagents flow completely into the lower reaction chamber, but for Reactor B some 5-(2-bromoethyl)phenanthridinium bromide solution remains unreacted after mixing because of the smaller volume of the reaction chamber. Hence, the dimensions of the reactionware control the outcome of the reaction.

reactors and in terms of the chemistry that could be performed within them) and the countless different architectures that could be created by robocast 3D printing, the synergy between vessel geometry and the chemistry that takes place inside could become an important new reaction parameter to be optimized and utilized in 3D-printed reactors. In other words, 3D-printed reactionware gives almost limitless control to the user in terms of creating bespoke reactionware: there is much more scope for creativity compared to that with traditional glassware. This is true in terms of both what the reactionware is made from and the types of reactionware that can be made. With regard to the latter, this freedom in 3D-printed reactionware architecture presents the user with both new questions and new solutions when attempting chemical discovery. One such question, which chemists rarely ask themselves, relates to finding the optimal reactor geometry for a desired chemical outcome. Such concepts could be very useful for optimizing reactions in 3D-printed reactionware, and might even allow reaction outcomes to be dictated at the reactionware design stage.

To exemplify this possibility in a very simple way, we compared two reactor architectures similar to that shown in Fig. 1c (without inserted frits) to perform the reaction of one equivalent of 4-methoxyaniline with three equivalents of 5-(2-bromoethyl)phenanthridinium bromide in d_6 -DMSO in the presence of excess Et_3N (ref. 21). The reaction details and key reactor dimensions are shown in Fig. 6. In the case of Reactor A, the volume of the two upper solution-holding chambers was 4.7 ml and the volume of the sole mixing/reaction chamber below was 9.5 ml (see Supplementary Information and Supplementary Fig. S6 for technical details). The difference between specified chamber volumes as entered in the design software and the actual volumes of the final printed chambers was within 5% in all cases (see Supplementary Fig. S6). One holding chamber held the 4-methoxyaniline and Et_3N in 1 ml d_6 -DMSO, and the other held the 5-(2-bromoethyl)phenanthridinium bromide solution (3 ml, also in d_6 -DMSO). Mixing of these solutions in the lower reaction chamber was then induced using a vacuum line as before, and the product distribution was monitored by 1H NMR spectroscopy, which showed a >90% conversion of 4-methoxyaniline starting material to heterocycle 5 after 21 hours. As the volume of the lower reaction chamber (9.5 ml) exceeded the total volume of the reagent solutions (4 ml), all of the reagents were able to mix and react in the lower

chamber of the reactionware. No heterocycle 4 was observed in this reaction mixture²².

The reactor architecture was then changed to that of Reactor B, identical to Reactor A in every respect except for having a smaller reaction chamber volume of only 2 ml. All other parameters were kept constant (concentrations, solution volumes, etc.). This meant that only 1 ml of each solution in the holding chambers could fit inside the reaction chamber, that is the reactor architecture enforced a 1:1 ratio of 4-methoxyaniline to 5-(2-bromoethyl)phenanthridinium bromide, with the residual 2 ml of the 5-(2-bromoethyl)phenanthridinium bromide solution remaining unreacted in the upper holding chamber (from which, theoretically, it could be siphoned off for other reactions). Using the design Reactor B, the ratio of 4 to 5 obtained after 21 hours was 80:20, which indicates a complete reversal of selectivity by simply and solely altering the reactionware architecture. This simple example demonstrates how optimized reactor geometry can be used to influence reactant stoichiometry and hence the outcome of a chemical reaction, without changing any of the other parameters in the experiment or the instructions given to the ‘operator’. Hence, using this approach, some measure of control over the products formed in a given reaction can be encoded during the digital design of the 3D-printed reactionware, and reactionware geometry becomes another variable to be experimented with during optimization processes.

As a final example of the power of digitally designed reactionware to change the way chemistry is performed, we examined the possibility of printing catalysts into the structure of the reactionware itself. To this end, we thinned acetoxy silicone bathroom sealant with toluene, and then added Pd/C until a paste suitable for printing was formed (see Supplementary Information and Supplementary Figs S3 and S7). Reactors were then printed that had this catalyst-loaded polymer incorporated within their structures. Using this 3D-printed reactionware, we examined the catalytic hydrogenation of styrene to ethylbenzene using Et_3SiH as the hydrogen source, according to known procedure²⁷. When reactionware impregnated with Pd/C was used for the reaction, quantitative conversion of styrene to ethylbenzene was observed within 30 minutes at room temperature, as judged by 1H NMR spectroscopy. No leaching of Pd/C into the solution was apparent by eye. However, when reactionware made solely from acetoxy silicone polymer was used, no conversion to ethylbenzene was observed over a period of two hours (see Supplementary Fig. S4). This

simple example demonstrates that catalysts can be printed into the kind of digitally designed robocast reactionware described herein, and illustrates the vast scope for invention and discovery that such an approach provides.

Conclusions

In conclusion, we have demonstrated the production and utility of completely reusable and self-healing bespoke reactionware, which would be extremely difficult to realize without the aid of robocasting techniques. Although the chemistry chosen to exemplify this technology is relatively simple, the potential for printing reagents and active components into the reactors themselves has the power to be truly transformative. Digital technology was used to design and manufacture the active reactionware, to initiate reactions and to monitor reactions *in situ*, and so gives an alternative to the traditional passive-vessel approaches to doing chemistry. Hence, we optimized our initial designs to synthesize three previously unreported compounds, and also to dictate the outcome of a fourth reaction solely by judicious alteration of the reactor architecture.

In all cases, the ease of reactor design and production held distinct advantages over traditional techniques (for example, glassblowing) and the potential range of materials that can be printed has great promise for creating reactionware with in-built localized functionality (such as printing catalysts into certain parts of the reactionware). Using such methods, we believe that it should be feasible to create active reactors, that is 'reactionware' that has control over reagent-mixing sequences, flow rates and methods of purification built into the reactor design, and so combine the disciplines of synthetic chemistry, molecular modelling and chemical engineering in a low-cost, reconfigurable and highly accessible format.

Moreover, the low cost associated with reactionware production and optimization, as well as the self-contained nature of these devices, means that they could be deployed safely even in non-laboratory environments, which constitutes the first steps towards single-user designed and operated chemical engineering systems. Work to further integrate design software, printing hardware and control of chemical outcomes so that chemistry relevant to molecular nanotechnology²⁸, catalyst optimization²⁹, complex chemical processes^{30,31} and drug design³² can be explored using this platform is currently underway in our laboratories.

Methods

Details of synthetic protocols, full characterization of new compounds, figures of thermogravimetric analyses, crystallographic data and notes on and diagrams of the 3D-reactionware are given in the Supplementary Information. Two videos showing the assembly of the reactionware, crystallization of compound **1** (Supplementary Video S1) and the electrode reaction (Supplementary Video S2) are also available. The Standard Tessellation Language files, which give computational instructions for printing duplicates of the reactionware used in this work, are available from the authors.

Received 13 October 2011; accepted 23 February 2012;
published online 15 April 2012

References

- Marks, P., Campbell, M., Aron, J. & Lipson, H. 3D printing: second industrial revolution is under way (special report). *New Sci.* **2823**, 17–20 (2011).
- Geissler, M. & Xia, Y. Patterning: principles and some new developments. *Adv. Mater.* **16**, 1249–1269 (2004).
- Nakamura, M., Iwanaga, S., Henmi, C., Arai, K. & Nishiyama, Y. Biomaterials and biomaterials for future developments of bioprinting and biofabrication. *Biofabrication* **2**, 014110 (2010).
- Lee, K.-W., Wang, S., Dadsetan, M., Yaszemski, M. J. & Lu, L. Enhanced cell ingrowth and proliferation through three-dimensional nanocomposite scaffolds with controlled pore structures. *Biomacromolecules* **11**, 682–689 (2010).
- Hanson Shepherd, J. N. *et al.* 3D microperiodic hydrogel scaffolds for robust neuronal cultures. *Adv. Funct. Mater.* **21**, 47–54 (2011).
- Cohen, D. L., Malone, E., Lipson, H. & Bonassar, L. J. Direct freeform fabrication of seeded hydrogels in arbitrary geometries. *Tissue Eng.* **12**, 1325–1335 (2006).
- Stampf, J. & Liska, R. New materials for rapid prototyping applications. *Macromol. Chem. Phys.* **206**, 1253–1256 (2005).

- Ahn, B. Y. *et al.* Omnidirectional printing of flexible, stretchable, and spanning silver microelectrodes. *Science* **323**, 1590–1593 (2009).
- Therriault, D., White, S. R. & Lewis, J. A. Chaotic mixing in three-dimensional microvascular networks fabricated by direct-write assembly. *Nature Mater.* **2**, 265–271 (2003).
- Ilievski, F., Mazzeo, A. D., Shepherd, R. F., Chen, X. & Whitesides, G. M. Soft robotics for chemists. *Angew. Chem. Int. Ed.* **50**, 1890–1895 (2011).
- Hasegawa, T., Nakashima, K., Omatsu, F. & Ikuta, K. Multi-directional micro-switching valve chip with rotary mechanism. *Sensor. Actuat. A Phys.* **143**, 390–398 (2007).
- Vilbrandt, T., Pasko, A. & Vilbrandt, C. Fabricating nature. *Technoetic Arts* **7**, 165–174 (2009).
- Pearce, J. M. *et al.* 3-D printing of open source appropriate technologies for self-directed sustainable development. *J. Sustain. Develop.* **3**, 17–29 (2010).
- Yager, P. *et al.* Microfluidic diagnostic technologies for global public health. *Nature* **442**, 412–418 (2006).
- Cook, T. R. *et al.* Solar energy supply and storage for the legacy and nonlegacy worlds. *Chem. Rev.* **110**, 6474–6502 (2010).
- Gratson, G. M., Xu, M. & Lewis, J. A. Microperiodic structures: direct writing of three-dimensional webs. *Nature* **428**, 386 (2004).
- Lewis, J. A. Direct ink writing of 3D functional materials. *Adv. Funct. Mater.* **16**, 2193–2204 (2006).
- Moore, J. L., McCuiston, A., Mittendorf, I., Ottway, R. & Johnson, R. D. Behavior of capillary valves in centrifugal microfluidic devices prepared by three-dimensional printing. *Microfluid. Nanofluid.* **10**, 877–888 (2011).
- Fab@Home. The open-source personal fabricator project, <http://www.fabathome.org> (accessed 21/02/2012).
- Malone, E. & Lipson, H. Fab@Home: the personal desktop fabricator kit. *Rapid Prototyping J.* **13**, 245–255 (2007).
- Parenty, A. D. C., Smith, L. V., Pickering, A. L., Long, D.-L. & Cronin, L. General one-pot, three-step methodology leading to an extended class of *N*-heterocyclic cations: spontaneous nucleophilic addition, cyclization, and hydride loss. *J. Org. Chem.* **69**, 5934–5946 (2004).
- Richmond, C. J., Eadie, R. M., Parenty, A. D. C. & Cronin, L. Fine tuning reactivity: synthesis and isolation of 1,2,3,12b-tetrahydroimidazo[1,2-*f*]phenanthridines. *J. Org. Chem.* **74**, 8196–8202 (2009).
- Rhino3D, NURBS modeling for Windows, <http://www.rhino3d.com> (McNeel, Barcelona).
- Kataria, A. & Rosen, D. W. Building around inserts: methods for fabricating complex devices in stereolithography. *Rapid Prototyping J.* **7**, 253–261 (2001).
- Kortz, U., Savelieff, M. G., Bassil, B. S. & Dickman, M. H. A large, novel polyoxotungstate: [As(III)₆W₆₅O₂₁₇(H₂O)₇]²⁶⁻. *Angew. Chem. Int. Ed.* **40**, 3384–3386 (2001).
- Tanaka, N., Unoura, K. & Itabashi, E. Voltammetric and spectroelectrochemical studies of dodecamolybdophosphoric acid in aqueous and water–dioxane solutions at a gold-minigrid optically transparent thin-layer electrode. *Inorg. Chem.* **21**, 1662–1666 (1982).
- Mandal, P. K. & McMurray, J. S. Pd–C induced catalytic transfer of hydrogen with triethylsilane. *J. Org. Chem.* **72**, 6599–6601 (2007).
- Boyle, M. M. *et al.* Mechanised materials. *Chem. Sci.* **2**, 204–210 (2011).
- Maldonado, A. G. & Rothenberg, G. Predictive modeling in homogeneous catalysis: a tutorial. *Chem. Soc. Rev.* **39**, 1891–1902 (2010).
- Browne, K. P., Walker, D. A., Bishop, K. J. M. & Grzybowski, B. A. Self-division of macroscopic droplets: partitioning of nanosized cargo into nanoscale micelles. *Angew. Chem. Int. Ed.* **49**, 6756–6759 (2010).
- Cooper, G. J. T. *et al.* Modular redox active inorganic chemical cells: iCHELLs. *Angew. Chem. Int. Ed.* **50**, 10373–10376 (2011).
- Murphy, R. F. An active role for machine learning in drug development. *Nature Chem. Biol.* **7**, 327–330 (2011).

Acknowledgements

This work was supported by the Engineering and Physical Sciences Research Council UK via Creativity@HOME. L.C. thanks the Royal Society/Wolfson Foundation for a Merit Award. We thank R.M. Eadie (University of Glasgow) for samples of 2-bromoethylphenanthridinium bromide and E. Malone and K. Kondo (NextFab Studio, Philadelphia) for assistance with building the fabricator.

Author contributions

L.C. conceived the idea and organized the fabricator assembly, M.D.S., P.J.K., T.V., G.J.T.C. and R.W.B. designed the reactionware, M.D.S. and P.J.K. printed the devices, M.D.S., P.J.K., J.Y. and C.J.R. performed the experiments, L.C., M.D.S., P.J.K., J.Y. and C.J.R. analysed the results and M.D.S. and L.C. co-wrote the paper.

Additional information

The authors declare no competing financial interests. Supplementary information and chemical compound information accompany this paper at www.nature.com/naturechemistry. Reprints and permission information is available online at <http://www.nature.com/reprints>. Correspondence and requests for materials should be addressed to L.C.